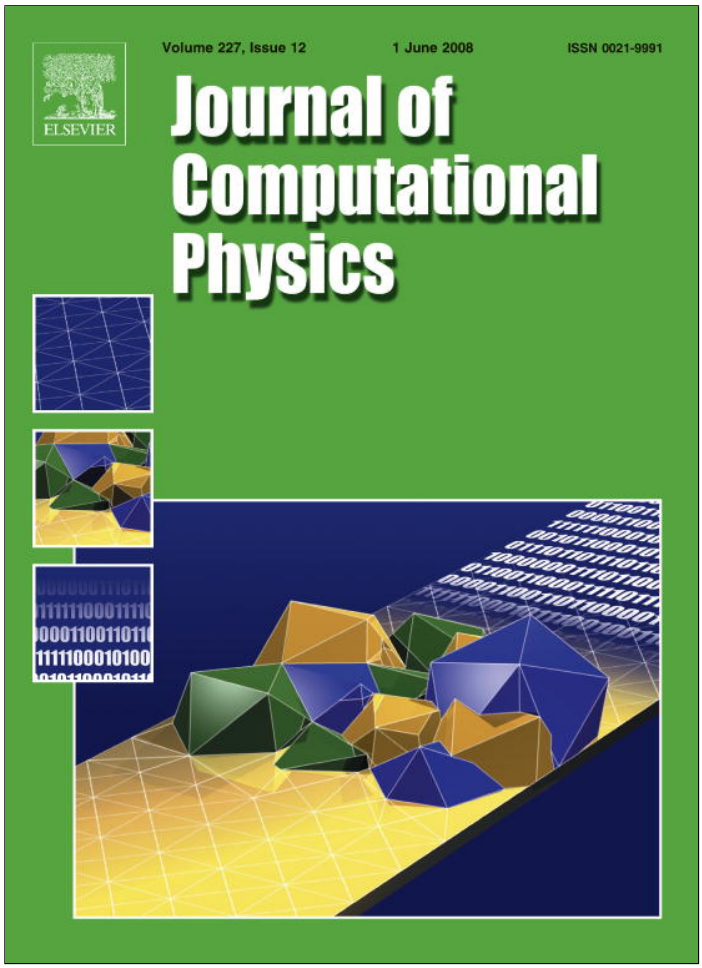

Available online at www.sciencedirect.com
ScienceDirect
Journal of Computational Physics 227 (2008) 6272–6287
JOURNAL OF COMPUTATIONAL PHYSICS
www.elsevier.com/locate/jcp

Application of the integro-moment method to steady-state two-dimensional rarefied gas flows subject to boundary induced discontinuities

Stelios Varoutis [a], Dimitris Valougeorgis [a,*], Felix Sharipov [b]

[a] Department of Mechanical and Industrial Engineering, University of Thessaly, Pedion Areos, Volos 38334, Greece
[b] Departamento de Física, Universidade Federal do Paraná, Caixa Postal 19044, Curitiba 81531-990, Brazil

Received 13 May 2007; received in revised form 30 January 2008; accepted 7 March 2008
Available online 16 March 2008

Abstract

The computational efficiency of the integro-moment method for solving steady-state two-dimensional rarefied gas flows is investigated. The two-dimensional boundary driven flow of a single gas in a cavity is used as a model problem, because the kinetic equations and the boundary conditions describing this flow contain most of the terms and features, which might appear in problems modeled by kinetic equations. Following a detailed quantitative comparison with the discrete velocity method, it is concluded that the integro-moment method may be considered as a alternative reliable and efficient computational scheme for solving rarefied (or non-equilibrium) flows in the whole range of the Knudsen number. Even more, it is shown that by implementing the integro-moment method the propagation of any discontinuities, which may exist at the boundaries, inside the computational domain and the production of an unphysical oscillatory behavior in the macroscopic quantities, are completely eliminated. The proposed integro-moment methodology is general and may be applied to any multidimensional non-equilibrium flow described by linear kinetic model equations.

Keywords: Rarefied gas flows; Boltzmann and kinetic model equations; Fredholm integral equations; Non-equilibrium flows; Knudsen number

1. Introduction

The simulation of rarefied gas flows in two and three dimensions requires the implementation of advanced computational approaches, which will provide accurate results with modest computational effort. The gas rarefaction is specified by the Knudsen number (Kn), which is defined as the ratio of the mean free path over a characteristic macroscopic length of the problem [1–4]. In general, when $Kn > 0.1$, the flow is considered as far from local equilibrium and then the well known hydrodynamic equations cannot be applied since the continuum assumption and the associated constitutive laws are not valid anymore. In these cases the problem

* Corresponding author. Tel.: +30 2421074058; fax: +30 2421074085.
E-mail address: diva@mie.uth.gr (D. Valougeorgis).

0021-9991/$ - see front matter © 2008 Elsevier Inc. All rights reserved.
doi:10.1016/j.jcp.2008.03.008

formulation is based on kinetic theory [1–3]. The unknown distribution function is obtained by solving the Boltzmann equation or its associated kinetic models, while the macroscopic quantities of practical interest are obtained by the moments of the distribution function. It is noted that in many occasions kinetic model equations are very reliable and can be used as an alternative to the Boltzmann equation producing accurate results with much less computational effort in the whole range of the *Kn* number. Typical examples are the BGK and S models for isothermal and non-isothermal flows respectively [4]. However, in general, the numerical solution of kinetic equations require significant computational effort.

One of the most commonly used computational methods for solving rarefied flows is the direct simulation Monte Carlo method (DSMC) [1]. This is a probabilistic approach, which actually circumvents the solution of the kinetic equations and over the years it has been found to be very efficient in solving high speed flows. In the case of flows characterized by small Mach numbers, the DSMC method suffers from statistical noise and looses its effectiveness. Despite some recent improvements the required computational time is drastically increased and it is very difficult to verify the accuracy of the results in several significant figures.

For low speed flows the kinetic equations can be linearized and then they can be solved in a straightforward manner by the discrete velocity method (DVM). This is a deterministic scheme, which has been extensively used over the years with considerable success in the solution of the Boltzmann equation [5–7] or of reliable kinetic models [8,4,9–12]. It is characterized by the discretization of the kinetic equations in the physical and molecular velocity spaces. The former is obtained by typical finite difference or finite volume schemes, while the latter by replacing the continuum spectrum of molecular velocities by a discrete set, which is properly chosen. Due to the discretization in the molecular velocity space the DVM is vulnerable to boundary induced discontinuities. In particular, when the flow problem is subject to boundary conditions with discontinuities then during the numerical estimation of the distribution functions, the discontinuities from the boundaries propagate inside the computational domain and produce an unphysical oscillatory behavior in the macroscopic quantities. This problem is well known as ray effects in the transport theory community and exists in neutron transport and radiative transfer [13], as well as in rarefied gas flows [14]. In the latter, the oscillatory behavior of the results starts as the Knudsen number departs from zero and it is increased by increasing the Knudsen number. The ray effects cannot be eliminated by simply increasing the number of discrete velocities since in this case the amplitude of the oscillations is decreased but their frequency is increased.

Although, methodologies have been proposed to eliminate this problem [15,16], it is obvious that the development and implementation of alternative computational schemes, which are not subject to ray effects, will be very useful. This need is also justified by the increased interest during the last years of solving rarefied gas flows in several emerging engineering and technological fields [17].

Such an alternative approach for handling low speed flows is the so-called integro-moment method (IMM). Basic information regarding the formulation and the characteristics of the method may be found in [2,4,18,19]. The basic advantage of the IMM is that the derived equations are discretized only in the physical space and no discretization in the molecular velocity space is needed. Therefore, due to its nature, the IMM is not subject to boundary induced discontinuities. Also, the IMM must not be confused with the classical moment method. Although in both methods the objective is to deduce a set of moment equations the two approaches are quite different. In particular, in the classical moment method the distribution function is assumed to be continuous in the velocity variables. Such an approximation is valid only at small Knudsen numbers and therefore the moment method provides reliable results only in the hydrodynamic and slip regimes. In addition, in the moment method a physical argument, which is not always fully justified, is required in order to close the system of governing equations. These pitfalls are circumvented in the formulation and implementation of the IMM. Over the years the IMM has been implemented mainly to problems in slab and axisymmetric geometries [20–28]. More recently, it has been demonstrated that the IMM can be applied to solve two-dimensional rarefied gas flows through channels of various cross sections [29,30]. However, this type of flow configurations, although are two-dimensional, they may be considered as a simple extension of the IMM, since the boundary conditions are continuous and only one moment of the distribution function is examined.

In the present work, the IMM is properly formulated to tackle two-dimensional problems, which are characterized by strong boundary discontinuities. In addition, the right hand side of the kinetic equation contains several moments of the distribution function and the boundary conditions are not homogeneous. As far as the authors are aware of there is only one attempt to handle this type of more complex rarefied flows using the

IMM [31]. It turns out that the extension of the IMM in such flow configurations, although in principal may look straightforward, it is not trivial. The proposed formulation is presented by using the two-dimensional flow of a single gas in a cavity, described by the linearized BGK equation [4,16], as a model problem. The kinetic equations and the boundary conditions describing the cavity flow problem contain all kind of terms, which might appear in problems modeled by kinetic equations and therefore it is used as a prototype problem. In addition, this particular problem has been recently solved by the DVM [16] and therefore we perform a detailed and systematic comparison of the two methods with regard to accuracy, convergence speed, storage and CPU time. This comparison yields some solid concluding remarks about the computational performance of the proposed IMM formulation and solution.

The formulation of the IMM is consisting, in general, of the following steps:

(i) The kinetic equation is solved on the basis of the method of characteristics and a closed form expression is obtained for the unknown distribution function in terms of the boundary conditions and the unknown macroscopic quantities.
(ii) This expression for the distribution function is substituted into the integral expressions for the macroscopic quantities to yield a set of coupled Fredholm integral equations.
(iii) When the boundary conditions contain unknown incoming distributions, following a similar procedure, a set of integral equations is derived for the unknown quantities at the boundaries.
(iv) The deduced system of integral equations is solved numerically.

It is important to note that although the IMM formulation is presented in two dimensions, its extension in three dimensions is straightforward. Also, the present analysis, which is based on the BGK equation is applicable to other linear kinetic models (e.g. S, ES, etc. [4]). It is obvious that as we advance from two to three dimensions and to more complex kinetic equations the required computational effort is increased. However, beyond that, there are no new difficulties or trouble issues, which have not been tackled and resolved here. Overall, it is argued that the proposed IMM procedure is general and can be applied to any multidimensional rarefied gas flow described by a system of linear integro-differential equations.

2. Model problem

The model problem is consisting of the isothermal flow of a rarefied gas in a two-dimensional cavity with rectangular cross section. Since a complete statement of the problem is provided in [16], here we present only a brief description and the basic equations governing the flow with the associated boundary conditions.

The flow domain, shown in Fig. 1, is restricted by $-1/2 \leqslant x \leqslant 1/2$ and $0 \leqslant y \leqslant A$, where A is the aspect ratio, defined as the ratio of the height over the width of the cavity. The flow is due to the motion of the wall at $y = A$. All lengths are in dimensionless form, by taking the width of the cavity as the characteristic length. Next, by assuming that the constant velocity U_0 of the moving wall is small compared to the most probable molecular speed v_0 ($U_0 \ll v_0$), the ratio U_0/v_0 is used as the small parameter to linearize the kinetic equation.

Then, the gas flow under investigation can be described by the linearized Bhatnagar, Gross, Krook (BGK) [4,16,32] equation

$$\mu\left[\cos\theta\frac{\partial\phi}{\partial x}+\sin\theta\frac{\partial\phi}{\partial y}\right]+\delta\phi=\delta[\rho+2\mu(u_x\cos\theta+u_y\sin\theta)], \tag{1}$$

where $\phi=\phi(x,y,\mu,\theta)$ is the unknown perturbation function, which depends on the spatial variables x and y and on the molecular velocity vector defined by its magnitude $0 \leqslant \mu < \infty$ and its polar angle $0 \leqslant \theta \leqslant 2\pi$. Here, the most probable speed v_0 is used as the unity of the molecular speed. The quantities at the right hand side of Eq. (1) are defined by the moments of ϕ according to

$$\rho(x,y)=\frac{1}{\pi}\int_0^{2\pi}\int_0^{\infty}\phi\mu e^{-\mu^2}\,d\mu\,d\theta, \tag{2}$$

$$u_x(x,y)=\frac{1}{\pi}\int_0^{2\pi}\int_0^{\infty}\phi\mu^2 e^{-\mu^2}\cos\theta\,d\mu\,d\theta, \tag{3}$$

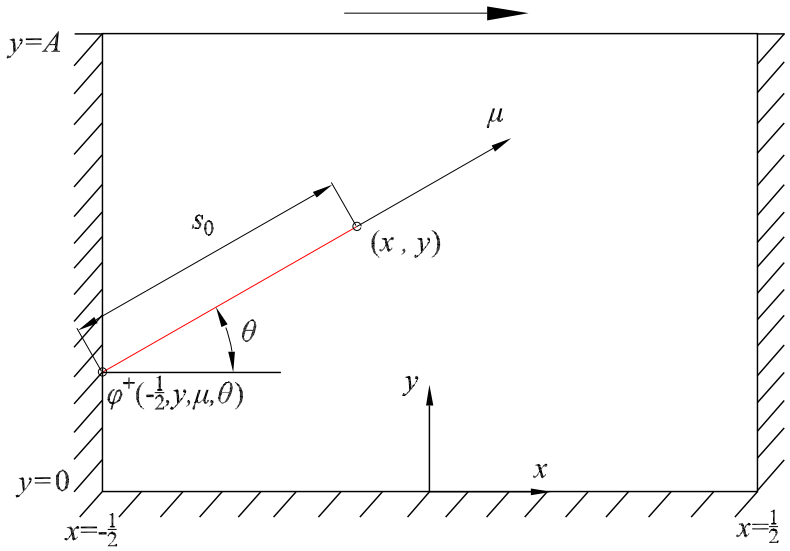

Fig. 1. Flow domain with the coordinate system and its origin and definition of the distance s_0 and the outgoing boundary distribution $\phi^+(-\frac{1}{2},y,\mu,\theta)$ along a typical characteristic s.

and

$$u_y(x,y)=\frac{1}{\pi}\int_0^{2\pi}\int_0^{\infty}\phi\mu^2 e^{-\mu^2}\sin\theta\,d\mu\,d\theta. \tag{4}$$

They represent the number density and the two components of the bulk velocity in the x and y direction, respectively. Another macroscopic quantity, which will be of interest in our work is the shear stress given by

$$\Pi(x,y)=\frac{1}{\pi}\int_0^{2\pi}\int_0^{\infty}\phi\mu^3 e^{-\mu^2}\sin\theta\cos\theta\,d\mu\,d\theta. \tag{5}$$

Finally, in Eq. (1), δ is the rarefaction parameter, which is proportional to the inverse Knudsen number and it is defined as

$$\delta=\frac{PW}{\eta v_0}=\frac{\sqrt{\pi}}{2}\frac{1}{Kn}, \tag{6}$$

where P is a reference gas pressure, W is the cavity width and η is the shear viscosity. For $\delta=0$ the flow is in the free molecular regime, while the case $\delta\to\infty$ corresponds to the hydrodynamic limit.

It is noted that in the governing Eq. (1) only the perturbations with respect to number density and velocity have been included, while the temperature perturbation term has been omitted. This is due to the fact that in previous work [16] it has been shown that the temperature variation in the flow field is very small and its impact on the major quantities of the flow of practical interest, such as velocity and shear stress distributions, is negligible.

Next, applying the Maxwell diffuse boundary conditions for the outgoing distributions at the boundaries [16] yields at the three stationary walls

$$\phi^+\left(-\frac{1}{2},y,\mu,\theta\right)=\rho_L\left(-\frac{1}{2},y\right)\quad\text{for}\quad -\frac{\pi}{2}\leqslant\theta\leqslant\frac{\pi}{2}, \tag{7}$$

$$\phi^+(x,0,\mu,\theta)=\rho_B(x,0)\quad\text{for } 0\leqslant\theta\leqslant\pi, \tag{8}$$

$$\phi^+\left(\frac{1}{2},y,\mu,\theta\right)=\rho_R\left(\frac{1}{2},y\right)\quad\text{for}\quad \frac{\pi}{2}\leqslant\theta\leqslant\frac{3\pi}{2}, \tag{9}$$

and at the moving wall ($y=A$)

$$\phi^+(x,A,\mu,\theta)=\rho_T(x,A)+2\mu\cos\theta\quad\text{for } \pi\leqslant\theta\leqslant 2\pi. \tag{10}$$

The superscript + denotes outgoing distributions at the boundaries and the parameters ρ_i, with $i = L, B, R, T$ denoting the left, bottom, right and top wall respectively, are estimated by applying the impermeability condition at each boundary to yield

$$\rho_L\left(-\frac{1}{2}, y\right) = -\frac{2}{\sqrt{\pi}} \int_{\frac{\pi}{2}}^{\frac{3\pi}{2}} \int_0^{\infty} \phi\left(-\frac{1}{2}, y, \mu, \theta\right) \mu^2 \mathrm{e}^{-\mu^2} \cos\theta \, \mathrm{d}\mu \, \mathrm{d}\theta, \tag{11}$$

$$\rho_B(x, 0) = -\frac{2}{\sqrt{\pi}} \int_{\pi}^{2\pi} \int_0^{\infty} \phi(x, 0, \mu, \theta) \mu^2 \mathrm{e}^{-\mu^2} \sin\theta \, \mathrm{d}\mu \, \mathrm{d}\theta, \tag{12}$$

$$\rho_R\left(\frac{1}{2}, y\right) = \frac{2}{\sqrt{\pi}} \int_{\pi}^{2\pi} \int_0^{\infty} \phi\left(\frac{1}{2}, y, \mu, \theta\right) \mu^2 \mathrm{e}^{-\mu^2} \cos\theta \, \mathrm{d}\mu \, \mathrm{d}\theta, \tag{13}$$

and

$$\rho_T(x, A) = \frac{2}{\sqrt{\pi}} \int_0^{\pi} \int_0^{\infty} \phi(x, A, \mu, \theta) \mu^2 \mathrm{e}^{-\mu^2} \sin\theta \, \mathrm{d}\mu \, \mathrm{d}\theta. \tag{14}$$

Thus, the model problem is described by the kinetic equation (1) and the associated integrals (2)–(4), subject to boundary conditions (7)–(10), which are supplemented by Eqs. (11)–(14). Our objective is to solve this problem in the whole range of δ and for any A via the IMM.

The model problem is subject to discontinuities at the four corners of the cavity, where the distribution function ϕ has two values coming from the corresponding boundary conditions. The discontinuities at the two corners connecting the moving and stationary walls is significantly stronger than in the other two corners due to the existence of the source term in the boundary condition (10). In addition, the outgoing distributions at the boundaries are not known and they are expressed in terms of the incident distributions, i.e. by Eqs. (11)–(14), which are part of the solution. Finally, the kinetic equation contains at its right hand side three moments of the unknown distribution. All these features make the model problem quite general covering most of the specific issues, which might appear in rarefied gas flows simulated by a kinetic approach. Therefore, the IMM formulation and numerical solution presented in the next two sections can be applied, in a straightforward manner, to a wide range of flows described by linearized kinetic equations.

3. Formulation of the integro-moment equations

Applying the method of characteristics we write Eq. (1) in the more convenient form

$$-\mu \frac{\mathrm{d}\phi}{\mathrm{d}s} + \delta\phi = \delta[\rho + 2\mu(u_x \cos\theta + u_y \sin\theta)], \tag{15}$$

where s denotes the distance from a point (x, y) along the characteristic defined by the polar angle θ of the molecular velocity vector. Then, multiplying (15) by $\exp(-\delta s/\mu)$ and integrating the resulting equation along the characteristic the following closed form expression for the unknown distribution function ϕ is deduced:

$$\phi(x, y, \mu, \theta) = \phi^+ \mathrm{e}^{-\delta s_0/\mu} + \frac{\delta}{\mu} \int_0^{s_0} [\rho(x', y') + 2\mu(u_x(x', y') \cos\theta + u_y(x', y') \sin\theta)] \mathrm{e}^{-\delta s/\mu} \mathrm{d}s. \tag{16}$$

Here, s_0 is the distance from a point (x, y) up to the boundary in the opposite direction to that of the molecular velocity (μ, θ), while ϕ^+ is the outgoing boundary distribution function where the characteristic terminates. The points (x', y') along the characteristic are related to the integration variables by

$$x' = x - s\cos\theta \quad \text{and} \quad y' = y - s\sin\theta. \tag{17}$$

A typical characteristic line s passing from a point (x, y) with a polar angle θ, along with the corresponding distance s_0 and boundary distribution ϕ^+, are shown in Fig. 1.

Eq. (16) is substituted into the integral expressions (2)–(4) to deduce, after some routine manipulation, three coupled integral equations for the macroscopic quantities of the number density and the x and y components of bulk velocity:

$$\rho(x,y) = \frac{\delta}{\pi}\int_0^{2\pi}\int_0^{s_0}\{T_0(\delta s)\rho(x',y') + 2T_1(\delta s)[u_x(x',y')\cos\theta + u_y(x',y')\sin\theta]\}\mathrm{d}s\,\mathrm{d}\theta + \frac{1}{\pi}\int_0^{2\pi} T_1(\delta s_0)\phi^+\,\mathrm{d}\theta, \tag{18}$$

$$u_x(x,y) = \frac{\delta}{\pi}\int_0^{2\pi}\int_0^{s_0}\{T_1(\delta s)\rho(x',y') + 2T_2(\delta s)[u_x(x',y')\cos\theta + u_y(x',y')\sin\theta]\}\cos\theta\,\mathrm{d}s\,\mathrm{d}\theta + \frac{1}{\pi}\int_0^{2\pi} T_2(\delta s_0)\phi^+\cos\theta\,\mathrm{d}\theta, \tag{19}$$

$$u_y(x,y) = \frac{\delta}{\pi}\int_0^{2\pi}\int_0^{s_0}\{T_1(\delta s)\rho(x',y') + 2T_2(\delta s)[u_x(x',y')\cos\theta + u_y(x',y')\sin\theta]\}\sin\theta\,\mathrm{d}s\,\mathrm{d}\theta + \frac{1}{\pi}\int_0^{2\pi} T_2(\delta s_0)\phi^+\sin\theta\,\mathrm{d}\theta. \tag{20}$$

Following the same procedure for the shear stress we readily find

$$\Pi(x,y) = \frac{\delta}{\pi}\int_0^{2\pi}\int_0^{s_0}\{T_2(\delta s)\rho(x',y') + 2T_3(\delta s)[u_x(x',y')\cos\theta + u_y(x',y')\sin\theta]\}\sin\theta\cos\theta\,\mathrm{d}s\,\mathrm{d}\theta + \frac{1}{\pi}\int_0^{2\pi} T_3(\delta s_0)\phi^+\cos\theta\,\mathrm{d}\theta. \tag{21}$$

The functions $T_a(z)$, with $a = 0, 1, 2, 3$, appearing in the kernel of Eqs. (18)–(21) belong to a class of transcendental functions defined by [33]

$$T_a(z) = \int_0^\infty c^a \exp\left(-c^2 - \frac{z}{c}\right)\mathrm{d}c. \tag{22}$$

The accurate estimation of the $T_a(z)$ functions is essential for the overall performance of the scheme and therefore the procedure for their estimation is presented in Appendix A. The outgoing boundary distributions ϕ^+, appearing in Eqs. (18)–(21), are given by the boundary conditions (7)–(10), depending on which of the four boundaries a characteristic line will terminate. Finally, the parameters ρ_i, with $i = L, B, R, T$ appearing in the boundary conditions are obtained by substituting (16) into Eqs. (11)–(14) to find

$$\rho_L\left(-\frac{1}{2},y\right) = -\frac{2\delta}{\sqrt{\pi}}\int_{\pi/2}^{3\pi/2}\int_0^{s_0}\{T_1(\delta s)\rho(x',y') + 2T_2(\delta s)[u_x(x',y')\cos\theta + u_y(x',y')\sin\theta]\}\cos\theta\,\mathrm{d}s\,\mathrm{d}\theta - \frac{2}{\sqrt{\pi}}\int_{\pi/2}^{3\pi/2} T_2(\delta s_0)\phi^+\cos\theta\,\mathrm{d}\theta, \tag{23}$$

$$\rho_B(x,0) = -\frac{2\delta}{\sqrt{\pi}}\int_{\pi}^{2\pi}\int_0^{s_0}\{T_1(\delta s)\rho(x',y') + 2T_2(\delta s)[u_x(x',y')\cos\theta + u_y(x',y')\sin\theta]\}\sin\theta\,\mathrm{d}s\,\mathrm{d}\theta - \frac{2}{\sqrt{\pi}}\int_{\pi}^{2\pi} T_2(\delta s_0)\phi^+\sin\theta\,\mathrm{d}\theta, \tag{24}$$

$$\rho_R\left(\frac{1}{2},y\right) = \frac{2\delta}{\sqrt{\pi}}\int_{-\pi/2}^{\pi/2}\int_0^{s_0}\{T_1(\delta s)\rho(x',y') + 2T_2(\delta s)[u_x(x',y')\cos\theta + u_y(x',y')\sin\theta]\}\cos\theta\,\mathrm{d}s\,\mathrm{d}\theta + \frac{2}{\sqrt{\pi}}\int_{-\pi/2}^{\pi/2} T_2(\delta s_0)\phi^+\cos\theta\,\mathrm{d}\theta, \tag{25}$$

and

$$\rho_T(x,A) = \frac{2\delta}{\sqrt{\pi}}\int_0^{\pi}\int_0^{s_0}\{T_1(\delta s)\rho(x',y') + 2T_2(\delta s)[u_x(x',y')\cos\theta + u_y(x',y')\sin\theta]\}\sin\theta\,\mathrm{d}s\,\mathrm{d}\theta + \frac{2}{\sqrt{\pi}}\int_0^{\pi} T_2(\delta s_0)\phi^+\sin\theta\,\mathrm{d}\theta. \tag{26}$$

The final set of coupled integro-moment equations to be solved is consisting of Eqs. (18)–(20) for the macroscopic quantities of number density and of the two components of the bulk velocity plus Eqs. (23)–(26) arising from the boundary conditions. Once this system of equations is solved and the quantities ρ, u_x and u_y are estimated, then the shear stress Π is obtained by Eq. (21).

4. Numerical scheme

The numerical solution of the system of integral Eqs. (18)–(20) and (23)–(26) may be obtained in several ways. Here, we propose a numerical scheme, which we have found to be very efficient and accurate.

In all equations, the double integrals require an integration over the whole computational domain, while the single integrals require an integration along the boundaries. The integration is performed by using the line-of-sight principal [21]. From Eq. (17), it is readily seen that

$$s = \sqrt{(x-x')^2 + (y-y')^2}, \quad \cos\theta = \frac{x-x'}{s} \quad \text{and} \quad \sin\theta = \frac{y-y'}{s}, \tag{27}$$

while

$$s\,\mathrm{d}s\,\mathrm{d}\theta = \mathrm{d}x'\,\mathrm{d}y'. \tag{28}$$

Based on the above transformation we write Eqs. (18)–(20) and Eqs. (23)–(26) in the more convenient and compact form

$$M_p(x,y) = \sum_{q=1}^{3} \int_0^A \int_{-1/2}^{1/2} U_{pq}(x,y:x',y') M_q(x',y')\,\mathrm{d}x'\,\mathrm{d}y' + \sum_{q=1}^{4} \int R_{pq}(x,y:\xi') L_q(\xi')\,\mathrm{d}\xi' + Q_p(x,y), \tag{29}$$

and

$$L_r(\xi) = \sum_{q=1}^{3} \int_0^A \int_{-1/2}^{1/2} V_{rq}(\xi:x',y') M_q(x',y')\,\mathrm{d}x'\,\mathrm{d}y' + \sum_{q=1}^{4} \int S_{rq}(\xi:\xi') L_q(\xi')\mathrm{d}\xi' + W_r(\xi), \tag{30}$$

respectively, where $p = 1,2,3$ and $r = 1,2,3,4$. Here,

$$M_1 = \rho, \quad M_2 = u_x \quad \text{and} \quad M_3 = u_y, \tag{31}$$

$$L_1 = \rho_L, \quad L_2 = \rho_B, \quad L_3 = \rho_R \quad \text{and} \quad L_4 = \rho_T, \tag{32}$$

while the kernels U_{pq}, V_{rq}, R_{pq} and S_{rq} and the source terms Q_p and W_r are given explicitly in the Appendix. In addition, when the integration is along the bottom and top boundaries then $\xi = x$ (and $\xi' = x'$), while when the integration is along the left and right boundaries then $\xi = y$ (and $\xi' = y'$). It is noted that all kernels are singular at $(x,y) = (x',y')$ and $(\xi = \xi')$.

We proceed with the discretization by dividing the computational domain in rectangular elements denoted by (i,j), with $i = 1,2,\ldots,I$ and $j = 1,2,\ldots,J$. The geometrical center of each element is determined by $x_i = (i-1/2)\Delta x$ and $y_j = (j-1/2)\Delta y$, $\Delta x = 1/I$ and $\Delta y = A/J$. The computational grid with a typical cell (i,j) and a typical boundary element k are shown in Fig. 2. Then, Eqs. (29) and (30) are approximated at each computational cell and each boundary segment as

$$M_p^{ij} = \sum_{q=1}^{3} \sum_{n=1}^{J} \sum_{m=1}^{I} U_{pq}^{ij,mn} M_q^{mn} + \sum_{q=1}^{4} \sum_{l=1}^{K} R_{pq}^{ij,l} L_q^l + Q_p^{ij}, \tag{33}$$

and

$$L_r^k = \sum_{q=1}^{3} \sum_{n=1}^{J} \sum_{m=1}^{I} V_{rq}^{k,mn} M_q^{nm} + \sum_{q=1}^{4} \sum_{l=1}^{K} S_{rq}^{k,l} L_q^l + T_r^k, \tag{34}$$

respectively, where $p = 1,2,3$, $r = 1,2,3,4$, $i = 1,2,\ldots,I$, $j = 1,2,\ldots,J$ and $k = 1,2,\ldots K$, while $K = I$ when the integration is along the bottom and top boundaries and $K = J$ when the integration is along the left and right boundaries. Even more, it is noted that

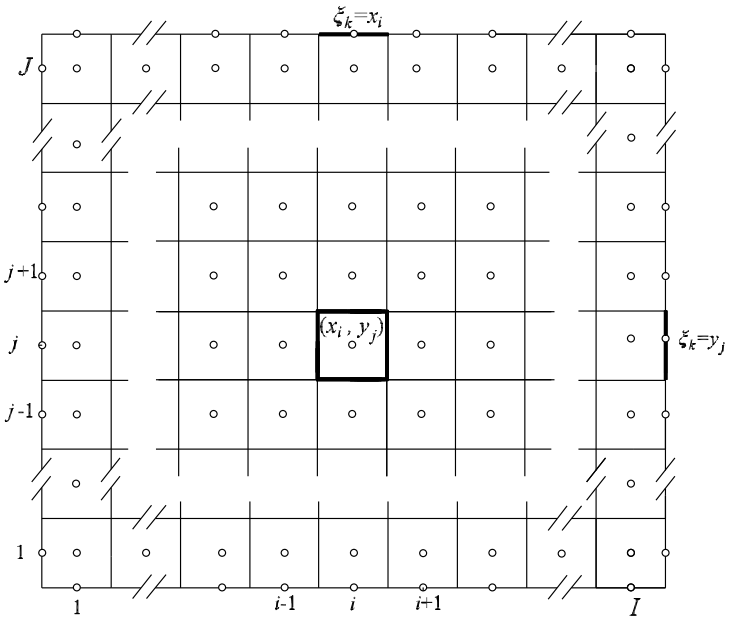

Fig. 2. Computational grid with typical cell and boundary elements.

$$M_p^{ij} = M_p(x_i, y_j), \quad M_q^{mn} = M_q(x_m, y_n) \quad \text{and} \quad Q_p^{ij} = Q_p(x_i, y_j), \tag{35}$$

$$L_r^k = L_r(\xi_k) \quad L_q^l = L_q(\xi_l) \quad \text{and} \quad W_r^k = W_r(\xi_k), \tag{36}$$

where $\xi_k = x_i$ ($\xi' = x'$) or $\xi_k = y_j$ ($\xi = y'$) depending upon the boundary that the integration takes place. Finally,

$$U_{pq}^{ij,mn} = \int_{y_n-\Delta y/2}^{y_n+\Delta y/2} \int_{x_m-\Delta x/2}^{x_m+\Delta x/2} U_{pq}(x_i, y_j : x', y')\mathrm{d}x'\,\mathrm{d}y', \tag{37}$$

$$V_{rq}^{k,mn} = \int_{y_n-\Delta y/2}^{y_n+\Delta y/2} \int_{x_m-\Delta x/2}^{x_m+\Delta x/2} V_{rq}(\xi_k, : x', y')\mathrm{d}x'\mathrm{d}y', \tag{38}$$

$$R_{pq}^{ij,l} = \int_{\xi_k-\Delta\xi/2}^{\xi_k+\Delta\xi/2} R_{pq}(x_i, y_j : \xi')\mathrm{d}\xi', \tag{39}$$

and

$$S_{rq}^{k,l} = \int_{\xi_k-\Delta\xi/2}^{\xi_k+\Delta\xi/2} S_{rq}(\xi_k : \xi')\mathrm{d}\xi'. \tag{40}$$

It is seen that the quantities M, Q in Eq. (33) and L, T in Eq. (34) are approximated by their corresponding values at the center of each cell and boundary segment respectively, while the quantities U, V and R, S are computed by integrating over each cell and along each boundary segment. Details on the estimation of the integrals (37)–(40), which depends only on geometrical parameters, are given in Appendix B.

Following the computation of the above integrals, Eqs. (33) and (34) are reduced into a system of algebraic equations and they are solved for the unknowns M_p^{ij} and L_r^k in an iterative manner. The iteration process starts by assuming initial estimates for M_q^{mn} and L_q^l at the right hand side of the equations and it is ended when the convergence criterion imposed on the overall quantities M is satisfied. Typical stationary or dynamic acceleration schemes may be applied to speed-up the convergence of the iteration scheme.

5. Results and discussion

The cavity flow problem has been solved via the IMM, implementing the proposed formulation and numerical scheme over a wide range of the rarefaction parameter δ and for various values of the aspect ratio A. In

particular, results are presented for $\delta = 0, 0.1, 1, 2, 5, 10$ and $A = 0.5, 1, 2$. For each set of these parameters three different computational grids are implemented, with $\Delta x = \Delta y = h$ in all cases. The absolute convergence criterion is equal to 10^{-7}.

The model problem, has been also solved by the discrete velocity method (DVM), which as pointed before is considered as the most efficient computational scheme for solving flows with small Mach and Reynolds numbers. Therefore, by comparing the corresponding results of the two methods it is possible to judge the computational effort as well as the expected accuracy of the IMM.

In order to have a first qualitative picture of the IMM results, some velocity streamlines for $A = 2$, and $\delta = 0, 1, 10$ are presented in Fig. 3, with $h = 0.01$. These flow patterns are identical with the ones obtained by the DVM and indicate that the proposed IMM is capable of capturing several flow configurations in a wide range of δ including the secondary vortices appearing under the main vortex as the rarefaction parameter δ is increased.

We proceed with a detailed quantitative study of the results. To achieve that we introduce two overall quantities namely the dimensionless flow rate G of the main vortex and the mean dimensionless shear stress D along the moving plate. The first quantity is defined by integrating the x-component of the velocity profile along the axis $x = 0$ from the center of the top vortex up to the moving wall of the cavity as

$$G = \int_O^A u_x(0, y)\mathrm{d}y, \tag{41}$$

where the point O denotes the center of the top vortex. The second quantity is obtained by integrating the shear stress along the moving wall of the cavity according to

$$D = \int_{-1/2}^{1/2} \Pi(x, A)\mathrm{d}x. \tag{42}$$

Based on these overall quantities a detailed comparison between the IMM and the DVM is presented in Tables 1–3 for $A = 0.5$, 1 and 2, respectively. In each table results of G and D with the corresponding required number of iterations and overall CPU time are provided, for $0 \leqslant \delta \leqslant 10$ and for three different computational grids consisting of about 850, 5150 and 20 300 nodes. To achieve that we have for $A = 0.5$ and $A = 2$ grids with 41×21, 101×51 and 201×101 points and for $A = 1$ grids with 29×29, 71×71 and 143×143 points. The results are based on the same convergence criterion imposed on the iteration map of both methods. It is also noted that the number of discrete velocities in the DVM method is $N = 12800$, which is the smallest number of discrete velocities required to ensure convergence up to at least two significant figures. The same convergence requirement is imposed on the IMM scheme in order to have a reliable comparison between the two methods.

From these tables it can be seen that in all cases as the grid is refined the dimensionless flow rate and mean shear stress obtained by the IMM converge up to at least two significant figures. In general, in rarefied atmospheres, i.e. at $\delta \sim 1$, the convergence rate is faster than in continuum atmospheres, i.e. at $\delta \to \infty$. It may be deduced that when the IMM is implemented for small values of δ the grid may be coarse, while for large values of δ dense grids are important to achieve good accuracy. Next, it is noted that the IMM converged results are in very good agreement with the corresponding DVM converged results. In all cases the converged results of the two methods agree up to at least two significant figures within ± 1 to the last one. It may be concluded that the proposed IMM scheme is a reliable algorithm for solving this particular problem, providing results with very good accuracy.

In order to examine the involved computational effort of the IMM we compare between the two methods the required number of iterations and CPU time. It is clearly seen that in both methods the number of iterations is increased as δ is increased, while for each δ the required number of iterations for the IMM and the DVM is about the same. The convergence characteristics including the spectral radius of the DVM has been studied in detail in [10]. There is no similar study for the convergence rate of the IMM but Tables 1–3 clearly indicate that the spectral radius of the two iterative processes must be very close.

Since the number of iterations upon convergence for both methods is about the same it is obvious that the comparison in terms of required CPU time depends on the CPU time per iteration. It is well known that the CPU time for one DVM iteration is proportional to the product $I \times J \times N$, where $I \times J$ are the nodes of

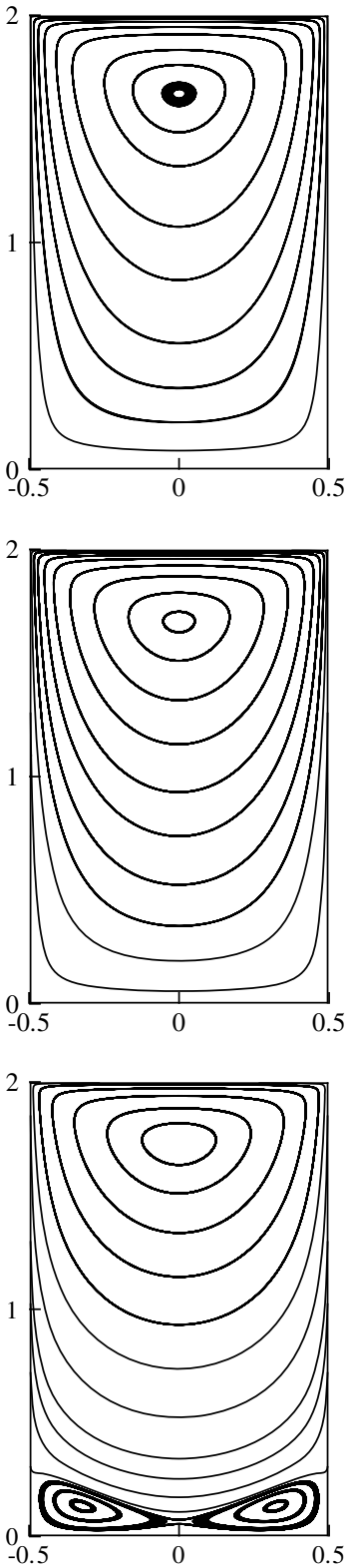

Fig. 3. Velocity streamlines for a cavity with $A = 2$ and $\delta = 0$ (top), $\delta = 1$ (middle) and $\delta = 10$ (bottom).

the grid and N the number of discrete velocities. Regarding the IMM, it is expected from the formulation of the method that the CPU time per iteration is proportional to $(I \times J)^2$. This finding is also verified by checking in Tables 1–3 the computational time with respect to the number of nodes at each of the three different grids. The CPU time of the IMM is less than the corresponding time of the DVM when the nodes

Table 1
G and D vs rarefaction parameter δ by IMM and DVM at $A = 0.5$

δ	Grid ($x \times y$)	IMM				DVM			
		G	D	Iterations	CPU (s)	G	D	Iterations	CPU (s)
0	41×21	0.533(−1)	0.728	22	14	0.549(−1)	0.720	23	52
0.1		0.543(−1)	0.719	22	14	0.559(−1)	0.714	22	50
1		0.623(−1)	0.655	20	13	0.640(−1)	0.668	23	52
2		0.691(−1)	0.608	29	16	0.710(−1)	0.627	34	76
5		0.836(−1)	0.523	64	25	0.852(−1)	0.537	71	160
10		0.982(−1)	0.440	142	48	0.992(−1)	0.440	160	358
0	101×51	0.533(−1)	0.728	22	278	0.538(−1)	0.725	24	333
0.1		0.544(−1)	0.719	22	280	0.549(−1)	0.719	22	305
1		0.625(−1)	0.655	20	260	0.630(−1)	0.674	23	320
2		0.695(−1)	0.608	29	352	0.700(−1)	0.634	34	471
5		0.842(−1)	0.523	64	715	0.846(−1)	0.545	72	994
10		0.988(−1)	0.440	148	1586	0.991(−1)	0.448	162	2246
0	201×101	0.533(−1)	0.728	23	5193	0.536(−1)	0.727	24	1519
0.1		0.544(−1)	0.719	23	5199	0.546(−1)	0.721	23	1458
1		0.625(−1)	0.655	21	4765	0.628(−1)	0.676	23	1456
2		0.695(−1)	0.608	29	6502	0.698(−1)	0.635	34	2147
5		0.843(−1)	0.522	64	14100	0.845(−1)	0.546	73	4598
10		0.989(−1)	0.437	148	33572	0.990(−1)	0.450	162	10191

Table 2
G and D vs rarefaction parameter δ by IMM and DVM at $A = 1$

δ	Grid ($x \times y$)	IMM				DVM			
		G	D	Iterations	CPU (s)	G	D	Iterations	CPU (s)
0	29×29	0.964(−1)	0.685	24	16	0.980(−1)	0.671	25	54
0.1		0.973(−1)	0.677	23	16	0.989(−1)	0.665	21	46
1		0.104	0.625	19	15	0.106	0.620	23	50
2		0.111	0.584	28	17	0.113	0.580	35	76
5		0.127	0.502	71	30	0.128	0.493	83	181
10		0.143	0.417	176	60	0.145	0.397	194	423
0	71×71	0.964(−1)	0.685	24	301	0.971(−1)	0.678	25	320
0.1		0.973(−1)	0.678	24	302	0.980(−1)	0.674	22	300
1		0.104	0.625	20	261	0.105	0.628	22	300
2		0.111	0.584	28	343	0.112	0.588	36	488
5		0.127	0.501	71	787	0.128	0.504	82	1109
10		0.144	0.413	175	1860	0.145	0.411	198	2672
0	143×143	0.964(−1)	0.685	24	5878	0.967(−1)	0.683	26	1393
0.1		0.973(−1)	0.678	24	5882	0.976(−1)	0.676	22	1178
1		0.104	0.625	20	4936	0.105	0.631	22	1178
2		0.111	0.584	28	6830	0.112	0.592	36	1922
5		0.127	0.500	71	17012	0.128	0.507	82	4369
10		0.145	0.412	175	41638	0.145	0.415	199	10582

of the computational grid $I \times J$ are less than the number N of discrete velocities and vice versa. When $N = I \times J$, then it is expected that the required CPU time for the two methods will be about the same. At this point it is noted that as the rarefaction parameter δ is increased both methods require a larger number of nodes $I \times J$. In addition, the DVM at small δ requires a large number of discrete velocities, which may be gradually decreased as δ is increased. Based on the above it may be concluded that the IMM is computationally more efficient than the DVM for $\delta \leqslant 1$ and the other way around for $\delta > 1$.

We conclude this section by making some comments on the issue of the ray effects. In Fig. 4, the x-component of the velocity profile along the axis $x = 0$ is provided for a cavity with $A = 1$ and $\delta = 10^{-3}$, using both methods. It is seen that the DVM results are subject to an oscillatory behavior known as ray effects, which can

Table 3
G and D vs rarefaction parameter δ by IMM and DVM at $A = 2$

δ	Grid ($x \times y$)	IMM				DVM			
		G	D	Iterations	CPU (s)	G	D	Iterations	CPU (s)
0	21×41	0.104	0.674	34	17	0.106	0.655	36	80
0.1		0.104	0.668	33	17	0.107	0.650	24	54
1		0.110	0.622	19	13	0.112	0.608	21	47
2		0.115	0.583	27	16	0.118	0.570	34	76
5		0.129	0.502	71	27	0.134	0.483	82	183
10		0.144	0.421	184	57	0.151	0.390	201	450
0	51×101	0.104	0.675	34	404	0.105	0.667	36	500
0.1		0.105	0.668	33	395	0.105	0.662	23	320
1		0.110	0.622	20	260	0.110	0.620	21	292
2		0.116	0.583	27	333	0.116	0.582	34	472
5		0.130	0.500	71	793	0.131	0.498	84	1163
10		0.147	0.413	185	1981	0.148	0.407	206	2848
0	101×201	0.104	0.675	34	7074	0.104	0.671	36	2267
0.1		0.105	0.668	33	6877	0.105	0.665	24	1516
1		0.110	0.622	20	4249	0.110	0.623	21	1327
2		0.116	0.583	27	5260	0.116	0.587	34	2141
5		0.131	0.499	71	13788	0.131	0.503	85	5339
10		0.147	0.411	185	40863	0.147	0.412	208	13042

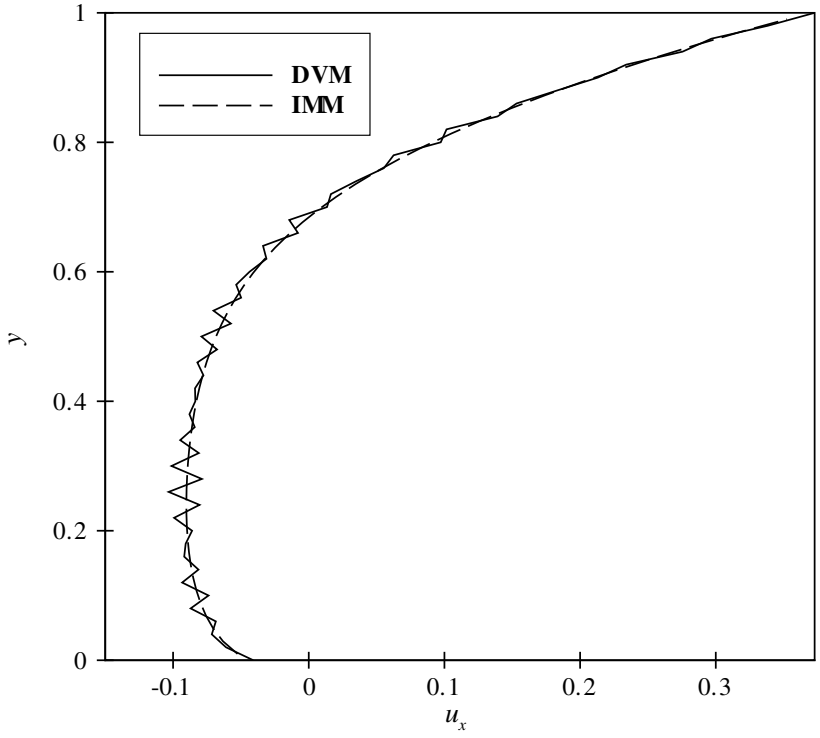

Fig. 4. Velocity profile of $u_x(0, y)$ for a cavity with $A = 1$ and $\delta = 10^{-3}$ by the *IMM* and *DVM*.

be eliminated only if the so-called splitting approach, as it has been done in [16], is applied. It is also seen that the IMM results are not subject to ray effects, since no discretization in the velocity space is needed.

6. Concluding remarks

The integro-moment method has been properly formulated for solving multidimensional non-equilibrium gas flows described by linear integro-differential equations. The efficiency of the proposed algorithm has been

demonstrated by solving the two-dimensional cavity flow problem in the whole range of the Knudsen number. This particular flow problem has been considered as a prototype problem because it contains most of the features, which might appear in non-equilibrium flows simulated by a kinetic approach.

Following a detailed quantitative comparison with the discrete velocity method it is concluded that the integro-moment method may be considered as a reliable alternative computational scheme for solving linear non-equilibrium multidimensional flows. The method is particularly suitable for problems, which are subject to boundary induced discontinuities eliminating completely their propagation inside the computational field and producing macroscopic results without oscillatory behavior. The present methodology with the associated computational scheme may be applied to other linear kinetic models describing rarefied gas flows in multidimensional geometries. At the present time, when the interest in the simulation of non-equilibrium problems has been significantly increased it is important to have various numerical methodologies for tackling such problems.

Acknowledgement

Partial support of this work by the Association Euratom – Hellenic Republic and by the Conselho Nacional de Desenvolvimento Cientifico e Tecnologico (CNPq, Brazil) is gratefully acknowledged. The views and opinions expressed here in do not necessary reflect those of the European Union.

Appendix A. Numerical estimation of the T_a functions

The estimation of the $T_a(x)$ functions, with $a = -1, 0, 1, 2, 3$, is performed numerically by applying a Gauss–Legendre quadrature. No recurrence relations have been used. The transformation

$$z(x) = \frac{x-1}{x+1} \tag{43}$$

is applied to map $x \in [0, \infty)$ onto $z \in [-1, 1]$. In all tabulated results of the present work a 64 point Gauss–Legendre quadrature has been implemented. This specific quadrature provides accurate estimates of the $T_a(x)$ functions up to seven significant figures within ± 1 in the last one. The accuracy of these estimates has been validated in several ways including a comparison with the corresponding results obtained by convergent series expansions [34,4].

Appendix B. Details in the numerical scheme

The kernels U_{pq}, V_{rq}, R_{pq} and S_{rq} and the source terms Q_p and W_r in Eqs. (29) and (30) are defined as follows:

$$U_{pq} = \frac{\delta}{\pi}\frac{1}{s}\begin{Bmatrix} T_0 & 2T_1\cos\theta & 2T_1\sin\theta \\ T_1\cos\theta & 2T_2\cos^2\theta & 2T_2\cos\theta\sin\theta \\ T_1\sin\theta & 2T_2\cos\theta\sin\theta & 2T_2\sin^2\theta \end{Bmatrix}, \tag{44}$$

$$V_{rq} = \frac{2\delta}{\sqrt{\pi}}\frac{1}{s}\begin{Bmatrix} -T_1\cos\theta & -2T_2\cos^2\theta & -2T_2\cos\theta\sin\theta \\ -T_1\sin\theta & -2T_2\cos\theta\sin\theta & -2T_2\sin^2\theta \\ T_1\cos\theta & 2T_2\cos^2\theta & 2T_2\cos\theta\sin\theta \\ T_1\sin\theta & 2T_2\cos\theta\sin\theta & 2T_2\sin^2\theta \end{Bmatrix}, \tag{45}$$

$$R_{pq} = \frac{1}{\pi}\frac{1}{s}\begin{Bmatrix} T_1 & T_1 & T_1 & T_1 \\ T_2\cos\theta & T_2\cos\theta & T_2\cos\theta & T_2\cos\theta \\ T_2\sin\theta & T_2\sin\theta & T_2\sin\theta & T_2\sin\theta \end{Bmatrix}, \tag{46}$$

$$S_{rq} = \frac{2}{\sqrt{\pi}}\frac{1}{s}T_2\begin{Bmatrix} -\cos\theta & -\cos\theta & -\cos\theta & -\cos\theta \\ -\sin\theta & -\sin\theta & -\sin\theta & -\sin\theta \\ \cos\theta & \cos\theta & \cos\theta & \cos\theta \\ \sin\theta & \sin\theta & \sin\theta & \sin\theta \end{Bmatrix}, \tag{47}$$

$$Q_p = \frac{2}{\pi}\frac{1}{s}\begin{Bmatrix} T_2\cos\theta \\ T_3\cos^2\theta \\ T_3\cos\theta\sin\theta \end{Bmatrix}, \tag{48}$$

$$W_r = \frac{4}{\sqrt{\pi}}\frac{1}{s}T_3\begin{Bmatrix} -\cos^2\theta \\ -\cos\theta\sin\theta \\ \cos^2\theta \\ 0 \end{Bmatrix}. \tag{49}$$

For convenience, the above quantities are given in terms of (s,θ) and they can be easily expressed in terms of (x,y,x',y') by using the relations in Eq. (27), while the functions $T_a = T_a(\delta s)$, with $a = 0,1,2,3$ are given by Eq. (22).

Next, we comment on the estimation of the integrals given by Eqs. (37)–(40). In particular, the double integrals (37) and (38) over the rectangular cell

$$x_m - \frac{\Delta x}{2} \leqslant x' \leqslant x_m + \frac{\Delta x}{2}, \quad y_n - \frac{\Delta y}{2} \leqslant y' \leqslant y_n + \frac{\Delta y}{2} \tag{50}$$

can be reduced into single integrals in an analytical manner if the integration over (x',y') is transformed in polar coordinates (s,θ). For demonstration purposes, let us consider the specific case of $U_{11}^{ij,mn}$, then the mathematical manipulation is as follows:

$$\begin{aligned} U_{11}^{ij,mn} &= \frac{\delta}{\pi}\int\int\frac{T_0(\delta s)}{s}\mathrm{d}x'\,\mathrm{d}y' = \frac{\delta}{\pi}\int\int T_0(\delta s)\mathrm{d}s\,\mathrm{d}\theta = \frac{1}{\pi}\int[T_1(0) - T_1(\delta s^*)]\mathrm{d}\theta \\ &= -\frac{1}{\pi}\int_{\theta_1}^{\theta_2} T_1\left(\delta\frac{x_i - x_m - \Delta x/2}{\cos\theta}\right)\mathrm{d}\theta - \frac{1}{\pi}\int_{\theta_2}^{\theta_3} T_1\left(\delta\frac{y_j - y_n - \Delta y/2}{\sin\theta}\right)\mathrm{d}\theta \\ &\quad -\frac{1}{\pi}\int_{\theta_3}^{\theta_4} T_1\left(\delta\frac{x_i - x_m + \Delta x/2}{\cos\theta}\right)\mathrm{d}\theta - \frac{1}{\pi}\int_{\theta_4}^{\theta_1} T_1\left(\delta\frac{y_j - y_n + \Delta y/2}{\sin\theta}\right)\mathrm{d}\theta. \end{aligned} \tag{51}$$

The distances $s^*(\theta)$ and the angles

$$\begin{aligned} \theta_1 &= \arctan\left(\frac{y_j - y_n + \Delta y/2}{x_i - x_m - \Delta x/2}\right), \quad \theta_2 = \arctan\left(\frac{y_j - y_n - \Delta y/2}{x_i - x_m - \Delta x/2}\right), \\ \theta_3 &= \arctan\left(\frac{y_j - y_n - \Delta y/2}{x_i - x_m + \Delta x/2}\right), \quad \theta_4 = \arctan\left(\frac{y_j - y_n + \Delta y/2}{x_i - x_m + \Delta x/2}\right) \end{aligned} \tag{52}$$

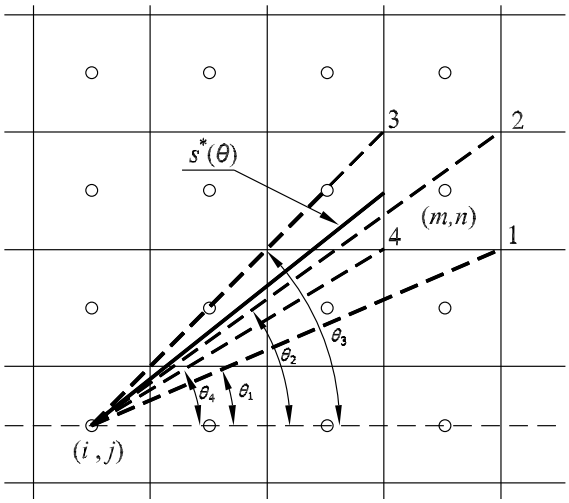

Fig. 5. Geometrical interpretation of $s^*(\theta)$ and of angles θ_1, θ_2, θ_3 and θ_4.

are shown in Fig. 5. In the case of $i = n$ and $j = m$, then

$$U_{11}^{ij,ij} = 1 - 4\int_0^{\pi/4} T_1\left(\delta\frac{\Delta x/2}{\cos\theta}\right)\mathrm{d}\theta - 4\int_{\pi/4}^{\pi/2} T_1\left(\delta\frac{\Delta y/2}{\sin\theta}\right)\mathrm{d}\theta. \tag{53}$$

This manipulation is applied to all $U_{pq}^{ij,mn}$ and $V_{pq}^{ij,mn}$. In the general case the reduction procedure is of the form

$$\delta\int\int(\cdot)\frac{T_a(\delta s)}{s}\mathrm{d}x'\mathrm{d}y' = \delta\int\int(\cdot)T_a(\delta s)\mathrm{d}s\,\mathrm{d}\theta = \frac{1}{\pi}\int(\cdot)[T_{a+1}(0) - T_{a+1}(\delta s^*)]\mathrm{d}\theta, \tag{54}$$

with $a = 0, 1, 2, 3$.

The deduced single integrals along with integrals (39) and (40), which are also calculated in terns of θ, are estimated numerically using the trapezoidal rule. It is noted that the analytical deduction of the double integrals into single integrals is important to upgrade the efficiency of the IMM in terms of accuracy and required CPU time.

References

[1] G.A. Bird, Molecular Gas Dynamics and the Direct Simulation of Gas Flows, Oxford University Press, Oxford, 1994.
[2] C. Cercignani, The Boltzmann Equation and its Application, Springer-Verlag, New York, 1988.
[3] J.H. Ferziger, H.G. Kaper, Mathematical Theory of Transport Processes in Gases, North-Holland Publishing Company, Amsterdam, 1972.
[4] F. Sharipov, V. Seleznev, Data on internal rarefied gas flows, J. Phys. Chem. Ref. Data 27 (3) (1998) 657–706.
[5] F.G. Tcheremissine, Conservative evaluation of the Boltzmann collision integral in discrete ordinates approximation, Comput. Math. Appl. 35 (1998) 215–221.
[6] V.V. Aristov, Direct Methods for Solving the Boltzmann Equation and Study of Nonequilibrium Flows, Kluwer Academic Publishers, Dordrecht, The Netherlands, 2001.
[7] S. Takata, S. Yasuda, S. Kosuge, K. Aoki, Numerical analysis of thermal-slip and diffusion-slip flows of a binary mixture of hard-sphere molecular gases, Phys. Fluids 15 (12) (2003) 3745–3766.
[8] D. Valougeorgis, Couette flow of a binary gas mixture, Phys. Fluids 31 (3) (1988) 521–524.
[9] F. Sharipov, Non-isothermal gas flow through rectangular microchannels, J. Micromech. Microeng. 9 (4) (1999) 394–401.
[10] D. Valougeorgis, S. Naris, Acceleration schemes of the discrete velocity method: gaseous flows in rectangular microchannels, SIAM J. Sci. Comput. 25 (2) (2003) 534–552.
[11] F. Sharipov, D. Kalempa, Gaseous mixture flow through a long tube at arbitrary Knudsen number, J. Vac. Sci. Technol. A 20 (3) (2002) 814–822.
[12] S. Naris, D. Valougeorgis, D. Kalempa, F. Sharipov, Flow of gaseous mixtures through rectangular microchannels driven by pressure, temperature and concentration gradients, Phys. Fluids 17 (10) (2005) 100607.1–100607.12.
[13] E.E. Lewis, W.F. Miller Jr., Computational Methods in Neutron Transport Theory, Wiley, 1984.
[14] Y. Sone, Sh. Takata, Discontinuity of the velocity distribution function in a rarefied gas around a convex body and the s layer at the bottom of the Knudsen layer, Transp. Theory Stat. Phys. 21 (4–6) (1992) 501–530.
[15] K. Aoki, C. Bardos, C. Dogbe, F. Golse, A note on the propagation of boundary induced discontinuities in kinetic theory, Math. Models Methods Appl. Sci. 11 (9) (2001) 1581–1595.
[16] S. Naris, D. Valougeorgis, The driven cavity flow over the whole range of the Knudsen number, Phys. Fluids 17 (9) (2005) 097106.
[17] J.M. Reese, M.A. Gallis, D.A. Lockerby, New direction in fluid mechanics: non-equilibrium aerodynamic and microsystem flows, Philos. Trans. R. Soc. London A 361 (2003) 2967–2988.
[18] M.N. Kogan, Rarefied Gas Dynamics, Plenum, New York, 1969.
[19] Y. Sone, in: D. Dini (Ed.), Rarefied Gas Dynamics, vol. 1, Editrice Tecnico Scientifica, Pisa, 1971, p. 737.
[20] C. Cercignani, C.D. Pagani, Variational approach to boundary value problems in kinetic theory, Phys. Fluids 9 (6) (1966) 1167–1173.
[21] P. Bassanini, C. Cercignani, F. Sernagiotto, Flow of a rarefied gas in a tube of annular section, Phys. Fluids 9 (6) (1966) 1174–1178.
[22] C. Cercignani, F. Sernagiotto, Cylindrical Couette flow of a rarefied gas, Phys. Fluids 10 (1967) 1200–1204.
[23] Y. Sone, K. Yamamoto, Flow of a rarefied gas through a circular pipe, Phys. Fluids 11 (1968) 1672–1678.
[24] Y.P. Pao, Some boundary value problems in the kinetic theory of gases, Phys. Fluids 14 (1971) 2285–2290.
[25] V.G. Chernyak, B.T. Porodnov, P.E. Suetin, Rarefied gas flow through long tubes with accommodating wall at arbitrary Knudsen number, Zh. Tekh. Fiz. 43 (11) (1973) 2420–2426 (in Russian).
[26] P.E. Suetin, V.G. Chernyak, About the dependence of Poiseuille slip and thermal crpeep on interaction law of gaseous molecules with a boundary surface, Izv. SSSR. Mekh. Zhidkosti Gaza 6 (1977) 107–114 (in Russian).
[27] K.C. Lea, S.K. Loyalka, Motion of a sphere in a rarefied gas, Phys. Fluids 25 (1982) 1550–1557.
[28] F. Sharipov, D. Kalempa, Gas flow near a plate oscillating longitudinally with an arbitrary frequency, Phys. Fluids 19 (1) (2007) 017110.1–017110.10.
[29] K. Aoki, Numerical analysis of rarefied gas flows by finite-difference method, in: E.P. Muntz, D.P. Weaver, D.H. Campbell (Eds.), Rarefied Gas Dynamics, vol. 118, AIAA, Washington, DC, 1989, p. 297.

[30] S. Varoutis, D. Valougeorgis, F. Sharipov, The integro-moment method applied to two-dimensional rarefied gas flows, in: A.K. Rebrov, M.S. Ivanov (Eds), 25th Rarefied Gas Dynamics, Novosibirsk, Russia, 2007, pp. 1235–1240.
[31] K. Aoki, Numerical analysis of a flow induced in a rarefied gas between noncoaxial circular cylinders with different temperatures for the entire range of the Knudsen number, Phys. Fluids A 1 (2) (1989) 409–419.
[32] P.L. Bhatnagar, E.P. Gross, M.A. Krook, A model for collision processes in gases, Phys. Rev. 94 (1954) 511–525.
[33] M. Abramowitz, I.A. Stegun (Eds.), 9th ed., Handbook of Mathematical Functions with Formulas, Graphs and Mathematical Tables, Dover Publications, New York, 1972.
[34] R. Cole, C. Pescatore, Evaluation of the integral $\int_0^\infty t^n \exp(-t^2 - \frac{x}{t})\mathrm{d}t$, J. Comput. Phys. 32 (1979) 280–287.